USCIPI REPORT #1080

Annual Technical Report
Nonlinear Real-Time Optical Signal Processing

by

A.A. Sawchuk, T.C. Strand, and A.R. Tanguay, Jr.

June 1982

Signal and Image Processing Institute
UNIVERSITY OF SOUTHERN CALIFORNIA
Department of Electrical Engineering-Systems
3740 McClintock Avenue, Room 404
Los Angeles, CA 90089-2564 U.S.A.

Unclassified

SECURITY CLASSIFICATION OF THIS PAGE *(When Data Entered)*

REPORT DOCUMENTATION PAGE		READ INSTRUCTIONS BEFORE COMPLETING FORM
1. REPORT NUMBER USCIPI Report 1080	2. GOVT ACCESSION NO.	3. RECIPIENT'S CATALOG NUMBER
4. TITLE *(and Subtitle)* NONLINEAR REAL-TIME OPTICAL SIGNAL PROCESSING		5. TYPE OF REPORT & PERIOD COVERED Annual Technical Report 4-15-81 to 4-14-82
		6. PERFORMING ORG. REPORT NUMBER USCIPI 1080
7. AUTHOR(s) A.A. Sawchuk, T.C. Strand, and A.R. Tanguay, Jr.		8. CONTRACT OR GRANT NUMBER(s) AFOSR-81-0082
9. PERFORMING ORGANIZATION NAME AND ADDRESS Department of Electrical Engineering Image Processing Institute University of Southern California, L.A., CA 90089-0272		10. PROGRAM ELEMENT, PROJECT, TASK AREA & WORK UNIT NUMBERS
11. CONTROLLING OFFICE NAME AND ADDRESS Air Force Office of Scientific Research Bldg. 410, Bolling AFB Washington, D.C. 20332		12. REPORT DATE June 30, 1982 13. NUMBER OF PAGES 66
14. MONITORING AGENCY NAME & ADDRESS*(if different from Controlling Office)* as above		15. SECURITY CLASS. *(of this report)* Unclassified 15a. DECLASSIFICATION/DOWNGRADING SCHEDULE

16. DISTRIBUTION STATEMENT *(of this Report)*

The United States Government is authorized to reproduce and distribute reprints for Governmental purposes notwithstanding any copyright notation hereon.

17. DISTRIBUTION STATEMENT *(of the abstract entered in Block 20, if different from Report)*

18. SUPPLEMENTARY NOTES

19. KEY WORDS *(Continue on reverse side if necessary and identify by block number)*

Optical Information Processing
Nonlinear Optical Processing
Optical Computing
Light Valves

20. ABSTRACT *(Continue on reverse side if necessary and identify by block number)*

The results of a one year research program in nonlinear real-time optical signal processing are described. The goal of the program is to extend fast parallel nonlinear operations to optical processing systems with large time-bandwidth and space-bandwidth products. The research has concentrated on optical mode (VGM) liquid crystal real-time spatial light modulators. Parallel and twisted nematic liquid crystal light valve (LCLV) devices have been used as a nonlinear element in a feedback arrangement in the sequential logic system. A computer generated hologram fabricated on an e-beam system serves as a beam-

DD FORM 1 JAN 73 1473 EDITION OF 1 NOV 65 IS OBSOLETE

UNCLASSIFIED

SECURITY CLASSIFICATION OF THIS PAGE *(When Data Entered)*

steering interconnection element. A completely optical oscillator and frequency divider have been experimentally demonstrated. Research has continued on variable-grating mode (VGM) liquid crystal devices that perform local spatial frequency modulation as a function of the incident intensity. These devices can be used for nonlinear processing by selection and recombination of these spatial frequency components. These devices have many interesting physical effects with useful applications in both analog and numerical optical signal processing. Preliminary theoretical modeling work to explain these effects is given, and an improved implementation of the intensity level slice function with VGM devices has been demonstrated. The project was a joint effort between the University of Southern California Image Processing Institute (USCIPI) and the Hughes Research Laboratories (HRL), Malibu, California.

TABLE OF CONTENTS

ABSTRACT

The results of a one year research program in nonlinear real-time optical signal processing are described. The goal of the program is to extend fast parallel nonlinear operations to optical processing systems with large time-bandwidth and space-bandwidth products. The research has concentrated on optical sequential logic systems for parallel digital processing and on variable grating mode (VGM) liquid crystal real-time spatial light modulators. Parallel and twisted nematic liquid crystal light valve (LCLV) devices have been used as a nonlinear element in a feedback arrangement in the sequential logic system. A computer generated hologram fabricated on an e-beam system serves as a beamsteering interconnection element. A completely optical oscillator and frequency divider have been experimentally demonstrated. Research has continued on variable-grating mode (VGM) liquid crystal devices that perform local spatial frequency modulation as a function of the incident intensity. These devices can be used for nonlinear processing by selection and recombination of these spatial frequency components. These devices have many interesting physical effects with useful applications in both analog and numerical optical signal processing. Preliminary theoretical modeling work to explain these effects is given, and an improved implementation of the intensity level slice function with VGM devices has been demonstrated. The project was a joint effort between the

University of Southern California Image Processing Institute (USCIPI) and the Hughes Research Laboratories (HRL), Malibu, California.

1. RESEARCH OBJECTIVES AND PROGRESS

1.1 Introduction and Project Overview

This report summarizes the results of a one year research effort in performing nonlinear operations in optical signal processing and achieving operation in real time using various input transducers. This section contains an introduction, motivation for the work and an overview of the research program. This current research program has evolved from a previous four year AFOSR program (Grant No. AFOSR-77-3285) for real-time nonlinear optical processing.

The recent research described in this report and the previous program both address the need for signal processing systems that can perform high throughput parallel multi-dimensional operations on signals with large time-bandwidth and space-bandwidth products. In many of these applications, digital hardware is inadequate. In the previous program, the range of available optical software has been greatly broadened to include A/D conversion, level slicing and logarithmic filtering. As part of these programs, modifications have been made to existing liquid crystal light valve (LCLV) real-time spatial light modulators and new devices such as the variable grating mode (VGM) light valve have been developed. Another goal of this research has been to explore numerical optical computing using binary or residue arithmetic. In these systems, signals exist as

discrete levels rather than as analog signals. This new approach holds much promise for the future if real-time processing speed, accuracy, and flexibility can be maintained.

An article [1] written by research personnel supported under this grant has been recently completed summarizing the state-of-the-art of all techniques of nonlinear optical processing. This article contains extensive references. Three major techniques of optically implementing nonlinear point functions have been developed. They are: halftoning; direct nonlinear processing using the inherent characteristics of image detectors and transducers; and intensity-to-spatial frequency conversion. Application examples and real-time implementation of these techniques are described in the review papers. A brief summary of these methods is given in a previous report [2].

During this past year of research we have concentrated on optical sequential logic systems that directly rely on the input-output characteristics of LCLV devices, and on variable grating mode (VGM) devices and their applications.

Direct nonlinear optical functions can be achieved using the inherent transfer characteristics of an optical recording medium or real-time image transducer. With this type of nonlinear processing, there is no pulse-width modulation, intensity-to-spatial frequency conversion or other type of intermediate mechanism. Thus, these techniques offer the potential of simple systems that avoid the noise problems

associated with many optical filtering techniques and have much less stringent space-bandwidth product requirements than systems which must modulate the input data. Such systems can implement parallel combinatorial logic and, with the addition of feedback, parallel sequential logic. Section 1.2 of this report describes these results in detail.

Another convenient method of obtaining point nonlinearities is through intensity-to-spatial frequency conversion. The idea is to encode each resolution element of an image with a grating structure where the period and/or the orientation of the grating is a function of the image intensity at the point in question. Assuming certain sampling requirements are met, each intensity level of interest is uniquely assigned to a different point in Fourier space and all points with a given intensity in the image are assigned to the same point in Fourier space (assuming space-invariant operation is desired). Then a pure amplitude spatial filter can alter the relative intensity levels in an arbitrary way, and combination of the filtered components produces various nonlinear functions. Both continuous-level (analog) nonlinear functions and various numerical logic functions (binary or residue) are possible. This method relies on the behavior of variable-grating mode (VGM) liquid crystal real-time devices which have been developed under this AFOSR program. Section 1.3 of this report describes work on physical modeling, and measurements of VGM liquid crystal devices. The goal of this work is to improve their temporal response,

uniformity, lifetime, etc. Several new types of electrically and optically activated VGM devices have been constructed and evaluated. A greatly improved experimental realization of a real-time intensity level slice has been achieved and is described in section 1.4.

The overall program has been a joint cooperative effort between the University of Southern California (USC) group and the Hughes Research Laboratories (HRL) in Malibu, California. Each group has participated in the project together since its beginning in April 1981 and a separate progress report is being submitted by HRL as a companion to this report. Both groups have worked closely together in their particular areas of expertise toward the project goals.

1.2 Optical Sequential Logic

1.2.1 Introduction

There has been considerable work in recent years in developing optical systems that perform essentially digital processing functions. The reasons for this interest include extending the flexibility of optical processing systems and the possibility of using the parallel capabilities of optical systems for digital signal processing. The first steps in the digital/optical research included parallel A/D conversion and optical combinatorial logic implementation. Both of these have been demonstrated in real-time systems at USC [3,4]. The next step in this progression of experiments is to demonstrate the feasibility of optical sequential logic. Here the basic logic gates are interconnected in a circuit which generally includes some form of feedback. In this system the temporal response characteristics of the system become very important. We have developed an optical system which demonstrates the feasibility of optical sequential logic. In particular we have implemented a totally optical system which includes a clock driving a master-slave flip-flop.

The basic elements of a sequential logic system are a nonlinear element that performs the desired logic function and an interconnection system to route the outputs of the nonlinear device to the appropriate inputs.

In our system the nonlinear element is a liquid crystal light valve (LCLV). A typical input-output characteristic curve for a 45 degree twisted-nematic LCLV is shown in Fig. 1. The binary states 1 or 0 corresponding to the output of a logic gate can be represented by two intensity levels. The inputs to a logic gate can be optically superimposed to yield, in the case of two-input gates, either a 0, 1, or 2. This three-level signal is the input to the nonlinear element (Fig. 2a). By biasing and scaling this input as shown in Fig. 1, a logical NOR operation is obtained. Other functions such as XOR, AND, OR can be achieved by substituting other nonlinearities, as shown in Fig. 2b, and the technique is easily extended to multiple inputs. Typical input-output characteristic curves for a parallel-aligned LCLV, biased for NOR and XOR operations, are shown in Fig. 3. Different operations are selected by choosing the available system parameters to make the input-output characteristic approximate the corresponding ideal nonlinearity shown in Fig. 2b (for two-input gates). While an oscillatory LCLV characteristic is required for XOR and XNOR operations, a monotonic behavior is preferred for the other operations. Monotonicity may be obtained by using either a twisted-nematic LCLV or a parallel-aligned LCLV with an appropriate liquid crystal layer thickness. The accuracy with which the intensity input-output curve needs to approximate the corresponding ideal nonlinearity will be considered in sections 1.2.3 and 1.2.4.4.

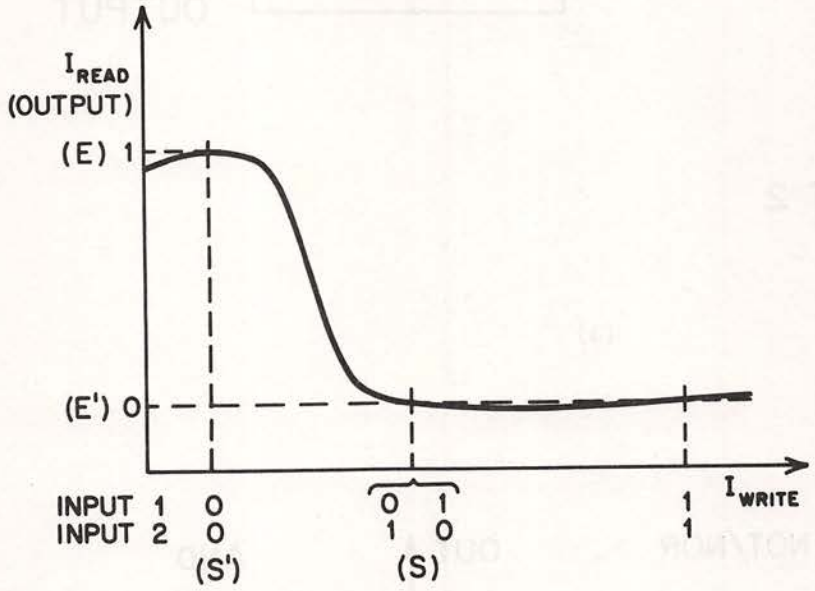

Fig. 1. Input-output characteristic of a twisted nematic LCLV, showing possible choice of levels for NOR operation.

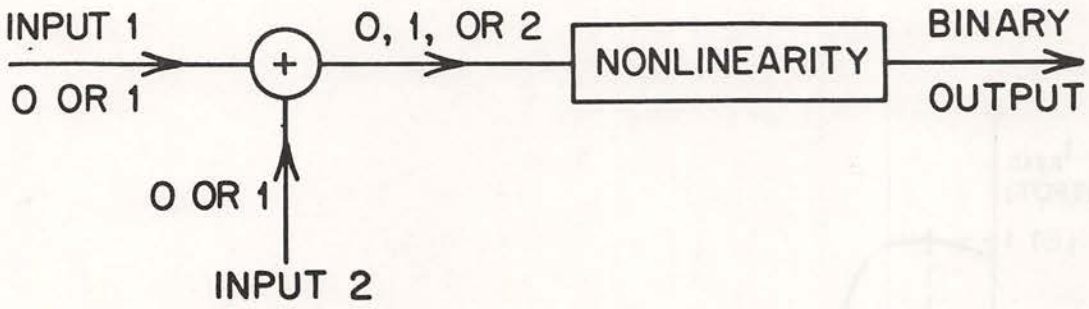

(a)

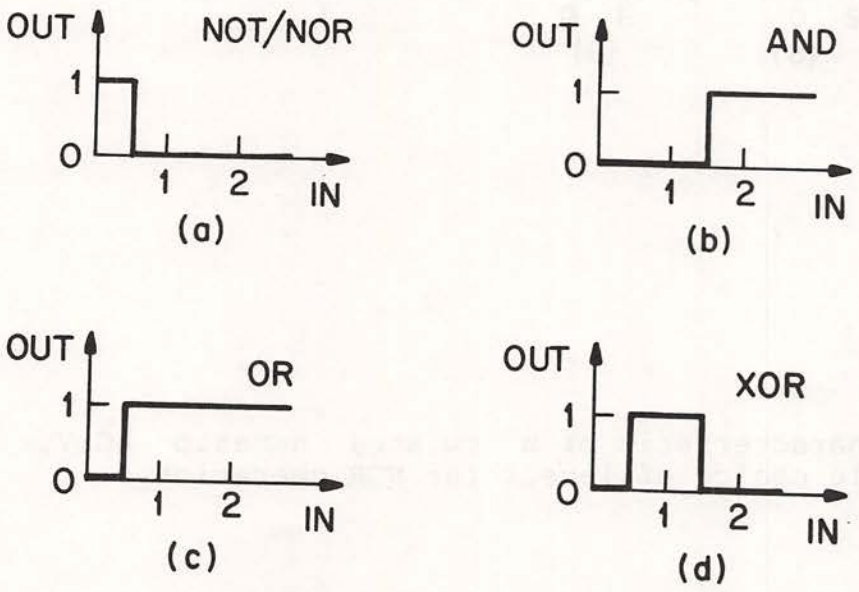

(b)

Fig. 2. (a) Implementation of a logic gate via an adder followed by a nonlinearity, and (b) possible choices of the nonlinearity to achieve Boolean operations.

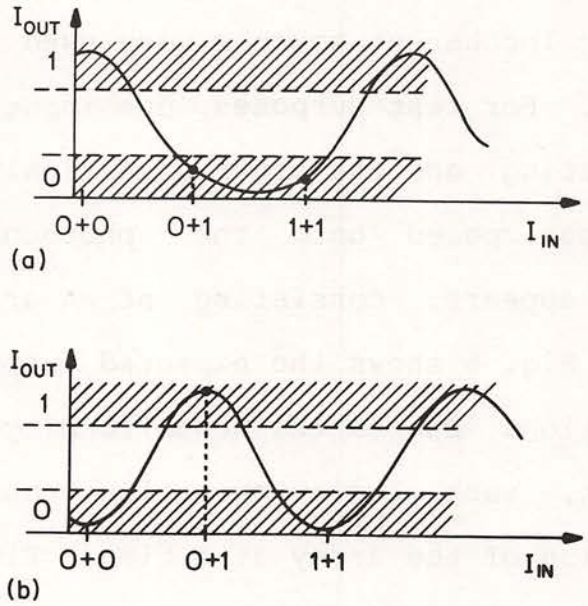

Fig. 3. Conceptual characteristic curves of the parallel-aligned LCLV showing (a) NOR operation and (b) XOR operation.

We have demonstrated these logic operations using a parallel-aligned LCLV. Incoherent sources were used for both the input and output beams. For test purposes, one input was chosen to be a horizontal grating, and the other a vertical grating, so that after being superimposed onto the photoconductor, a two-dimensional grid appears, consisting of an array of truth tables (Fig. 4). Thus Fig. 5 shows the expected output patterns for each logic operation. Due to the nonuniformity of the LCLV used in this experiment, each logic operation could only be performed over a portion of the array at a time. Figure 6 shows pictures of some sample outputs of the experimental system. The size of the grids pictured is on the order of two lines per millimeter at the LCLV. No attempt to determine the resolution limit of the LCLV was made. Given a uniform section of the LCLV, varying the available system parameters enabled all of the operations AND, NAND, OR, NOR, XOR, and XNOR to be performed. In general, however, the capability to implement all these logic operations is not necessary because they can all be built up from the NOR operation.

Both the static and dynamic response characteristics of the nonlinear element (LCLV) are critical in determining the operation of a sequential logic system. LCLV characteristics relevant to sequential logic are discussed in section 1.2.3.

The second major component of a sequential logic system is the interconnection network. An added advantage of optical

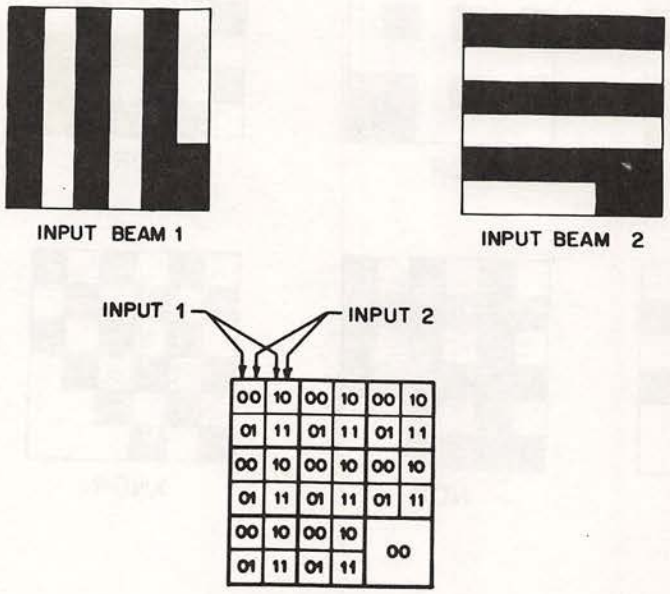

Fig. 4. Inputs for the combinatorial logic experiment with results of the superposition of the two inputs to generate truth tables.

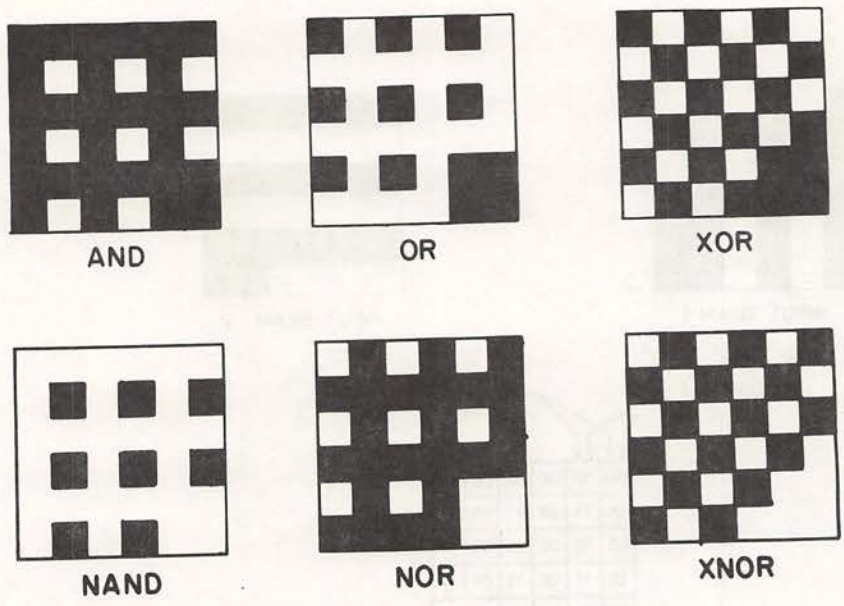

Fig. 5. Expected output for each logic operation. The lower-right corner of each output corresponds to an input of 0.

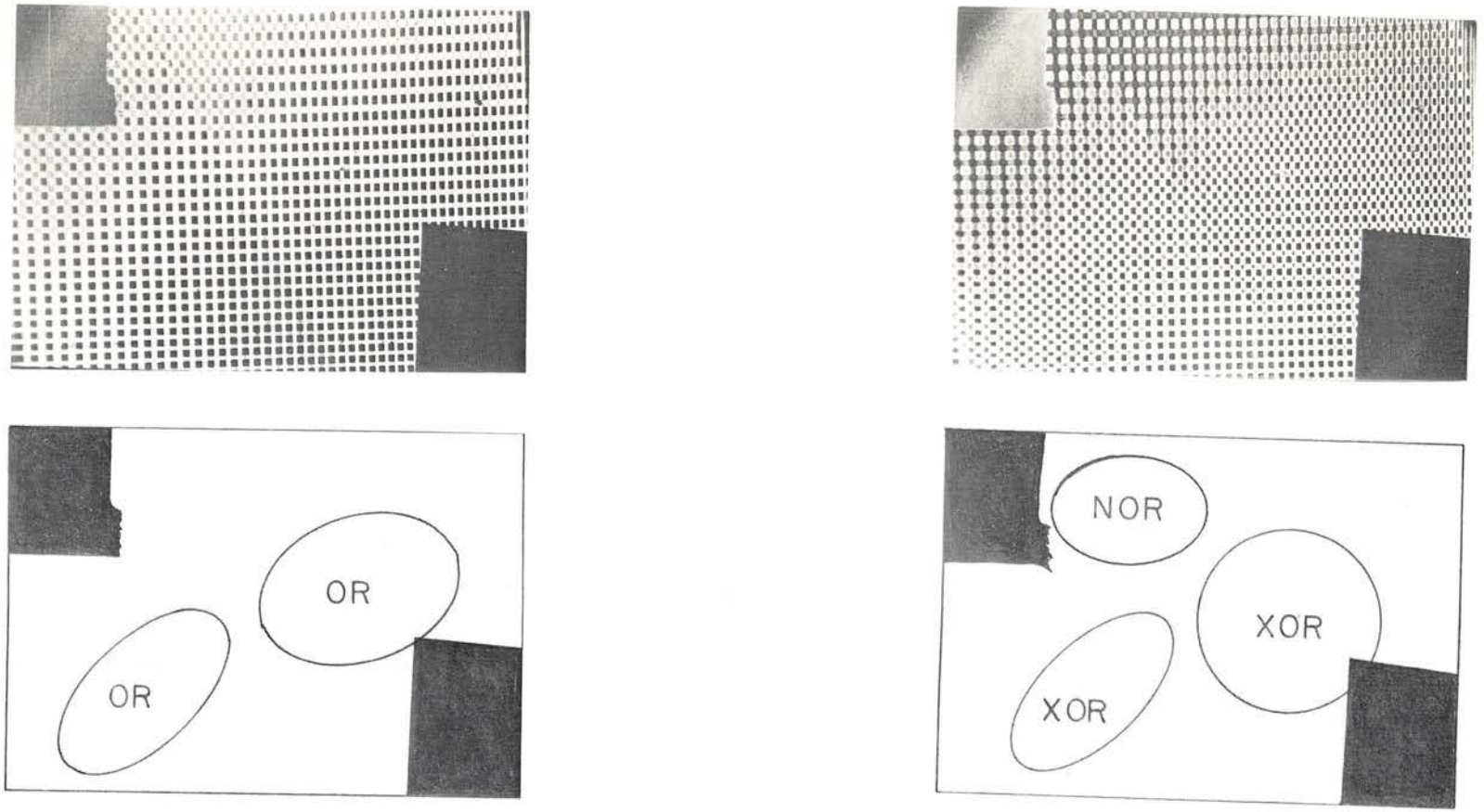

Fig. 6. Sample outputs of the combinatorial logic experiment. The lower left and upper right corners correspond to an input of 0.

systems over electronic ones is that the optical signals are largely immune to interference and cross-talk problems encountered when many different electrical signals are present in one system. There are many different possible techniques for guiding photons from one location to another which obviate the need for direct physical connections. In our method, computer generated holographic elements direct the signals to form the interconnection. With the current system there is a separate subhologram for each gate. The output from any given gate is imaged onto its corresponding subhologram. Each subhologram reconstructs a series of point images each of which is a gate input as shown in Fig. 7. The computer-generated hologram used for this work is described in section 1.2.2.

1.2.2 Interconnection Hologram

Many types of computer-generated, Fourier-transform holograms have been reported in the literature. Some of the more common ones include those introduced by Lohmann [5], Lee [6], Burckhardt [7], Hsueh and Sawchuk [8], and Fleuret [9]. For this type of application, the Fleuret hologram is the simplest, but it suffers from a low diffraction efficiency. Among the others, the efficiency is roughly the same whereas the Lee hologram has the best signal-to-noise ratio [10]. For these reasons, the Lee hologram is the most practical for use in this system.

The Lee hologram, like many others, encodes the Fourier transform of the desired object on the hologram. Since a

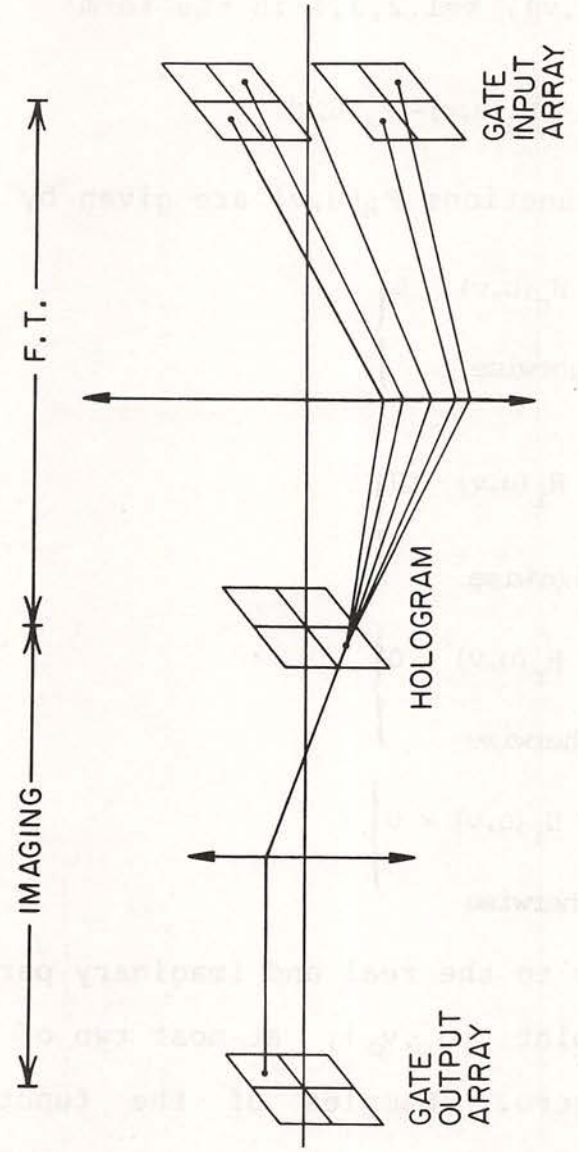

Fig. 7. Interconnection system using space-variant hologram.

hologram represents a complex-valued function, a means of encoding this function using only real nonnegative values must be used. The Lee method decomposes this function H(u,v) into four real nonnegative functions, $F_k(u,v)$, k=1,2,3,4 in the form

$$H(u,v) = F_1(u,v) + jF_2(u,v) - F_3(u,v) - jF_4(u,v) \tag{1}$$

where at each point (u,v), the functions $F_k(u,v)$ are given by

$$F_1(u,v) = \begin{cases} H_r(u,v) & \text{IF } H_r(u,v) > 0 \\ 0 & \text{otherwise} \end{cases} \tag{2}$$

$$F_2(u,v) = \begin{cases} H_i(u,v) & \text{IF } H_i(u,v) > 0 \\ 0 & \text{otherwise} \end{cases} \tag{3}$$

$$F_3(u,v) = \begin{cases} -H_r(u,v) & \text{IF } H_r(u,v) < 0 \\ 0 & \text{otherwise} \end{cases} \tag{4}$$

$$F_4(u,v) = \begin{cases} -H_i(u,v) & \text{IF } H_i(u,v) < 0 \\ 0 & \text{otherwise} \end{cases} \tag{5}$$

and the subscripts r and i refer to the real and imaginary parts, respectively. At a given point (u_o,v_o), at most two of the functions $F_k(u_o,v_o)$ will be nonzero. Samples of the function H(u,v) are then represented by cells on the hologram, each of which is divided into four subcells of equal size, one for each function $F_k(u,v)$ as shown in Fig. 8. Centered in each subcell is an aperture whose width is equal to the subcell width and whose height is proportional to the value of the appropriate function

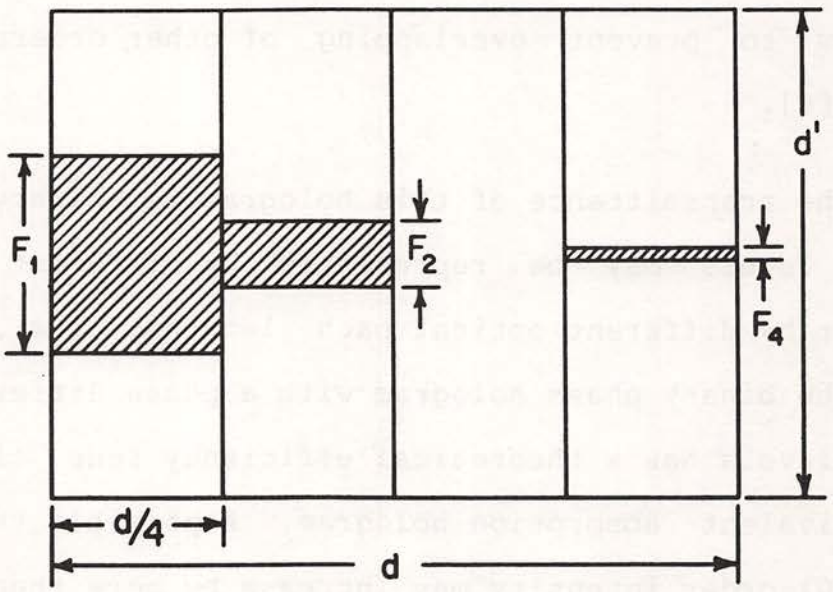

Fig. 8. Resolution cell of the Lee computer-generated hologram. Usually d=d'.

$F_k(u,v)$ at the center of that subcell. In each cell, the leftmost subcell represents F_1, the next subcell represents F_2, and so on through F_4. Upon reconstruction, the Fourier transform is taken with a lens, and the desired reconstruction appears in the (1,0) order, providing care has been taken in construction of the hologram to prevent overlapping of other orders onto the (1,0) order [6].

Since the transmittance of this hologram is binary valued, the binary levels may be represented by different levels of absorption or by different optical path lengths, i.e., a phase hologram. The binary phase hologram with a phase difference of π between the levels has a theoretical efficiency four times that of the equivalent absorption hologram. A possible tradeoff is that the (0,0)-order intensity may increase by more than a factor of four.

The hologram may be written onto film using a Dicomed film recorder or similar device, or may be written onto photoresist using electron-beam lithography. The latter method can write holograms with a much larger space-bandwidth product. An electron-beam system was used to create the hologram for our test circuit. The device used has a step size of 0.125 μm and has written patterns with linewidths as small as 0.5 μm. It writes 1.024x1.024mm fields and can stitch them together to cover a maximum area of 4x4 inches. The device provides a far greater space-bandwidth product than was needed for our test circuit.

One absorption and two phase holograms of our test circuit were made. This discussion will focus on the phase holograms, which use surface relief of the photoresist to obtain the optical path length difference. Figure 9 shows some pictures of one subhologram, taken with a scanning electron microscope (SEM). Figure 9a shows an entire subhologram, whose diameter is 1.04 mm, and Fig. 9b shows a portion of it with a higher magnification. The rectangles are pits, the exterior of which is a layer of photoresist, and the interiors of which are just glass substrate. The other three pictures (Figs. 9c-9e) show close-ups of rectangle edges. The thickness of the photoresist is 1.25 μm and the edges are inclined at approximately 32 degrees with respect to the substrate normal. The pictures reveal that the photoresist is slightly rough near the edges but is otherwise quite smooth (except for an occasional defect). Defects are apparent on the glass but are too small to affect the optical quality. Linewidths down to approximately 1 micron were obtained.

Defining efficiency as the power in the desired reconstruction pixels due to one subhologram divided by the power incident on that subhologram, the maximum efficiency over all subholograms was measured to be 5%. The efficiencies of the other subholograms were intentionally reduced in order to normalize the intensities in the reconstruction plane. This measurement was taken using an illumination wavelength of 514.5 nm, the wavelength used in the sequential logic system.

This is close to the optimum wavelength for this hologram. Besides efficiency, we must consider the noise appearing in the desired reconstruction order, of which there are three sources: (1) the encoding process used to represent the complex-valued function on the hologram, (2) scattering from the photoresist and glass substrate, and (3) the tail of the (0,0) order. The pictures of Fig. 9 indicate that the contribution due to scattering should be small, and this is verified by experiment. The effect of the (0,0) order could be substantial with a phase hologram, but can be filtered out spatially if the location of the limiting aperture is chosen appropriately. This leaves the encoding process as the major source of noise. The effect of the encoding process on noise is discussed in Ref. [10]. Measurements on our test hologram indicate a signal-to-noise ratio of approximately 60.

1.2.3 Liquid Crystal Light Valve

Of primary importance in determining the performance of the sequential logic system is the behavior of the liquid crystal light valve (LCLV). This section covers both static and dynamic LCLV characteristics.

First the static characteristics will be considered. The input-output characteristic of the device is used to approximate the ideal transfer characteristic (e.g., Fig. 2b) for the operation being performed (e.g., NOR). The actual device curve may be varied by varying the applied bias voltage and the angle

of the LCLV relative to the incident polarization of the read beam. Some measure is needed to determine how closely a given curve approximates the ideal. Referring to a transfer curve for NOR operation (Fig. 1), input and output extinction ratios, R_i and R_o respectively, may be defined as

$$R_i = S/S' \tag{6}$$

$$R_o = E/E' \tag{7}$$

where S' and S are the intensity levels that correspond to input levels of 0 and 1 respectively, and E' and E are the percent reflectivities that correspond to output levels of 0 and 1 respectively (E' being the larger of the two possible 0-level outputs). The ratio R_o/R_i should be larger than 1 and can serve as a figure of merit. For the ideal curve $R_o = \infty$ and $R_i = 1$. Another important parameter is S/E, a measure of the overall sensitivity of the LCLV. When used in a sequential logic system, S/E must be less than or equal to the power available, I_s, defined as the intensity incident on the liquid crystal times the overall transmittance of the feedback loop.

The static transfer curve of the device was optimized by varying its orientation and bias voltage. The optimum curve yielded values:

$$R_o / R_i = 2.7 \ , \ S/E = 21 \ \mu W/cm^2.$$

For the experimental system used, I_s is greater than S/E when the

laser output power is larger than 420 mW. Thus the device satisfies the criteria for use in the sequential logic system.

The uniformity over the spatial extent of a given device must also be taken into account. Each point on the LCLV will give rise to a static input-output transfer curve. Figures of merit can then be derived from the worst case over all pixels that will be used in the system. Thus the figures of merit become

$$M_1 = \min \{R_o\} / \max \{R_i\} \tag{8}$$

$$M_2 = \max \{S\} / \min \{E\} \tag{9}$$

where each extremum is taken over all possible curves. Static transfer curves have been recorded at different locations on the device with all other parameters held constant. The device used in the uniformity measurements was actually a different device than was used in the logic experiment, although both devices were of the same type. Transfer curves are shown for the mean over all locations studied as well as for one standard deviation on each side of the mean (Fig. 10). The locations studied covered a linear region on the device of approximately 1.7 cm. The variations over this region are small enough to satisfy the above criteria.

Turning now to time-dependent behavior, measurements of the LCLV response to positive-going and negative-going intensity step

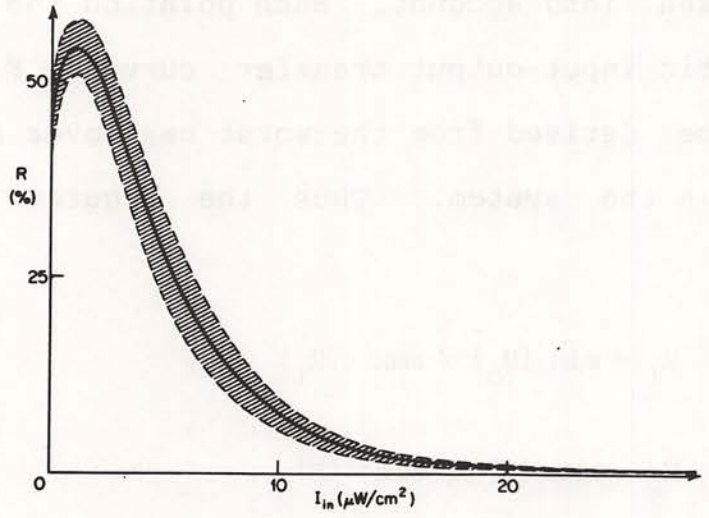

Fig. 10. Experimental range of transfer curves for LCLV device.

function inputs have been made. Sample responses are shown in Fig. 11. The fall (or rise) time is defined using the point on the temporal response that is 50% of the level at time $t \leq 0$ for a falling output (or 50% of the $t = \infty$ level for a rising output). The rise or fall time is then the absolute value of the reciprocal of the slope at that point. These temporal response measurements reveal that the rise time is much smaller than the fall time and that they both are a function of incident intensity and LCLV bias voltage. Furthermore, the LCLV response to a step input in bias voltage with a constant input intensity is much faster, indicating that the limiting element in the above temporal response is the photoconductor. Most of the nonlinearity of the LCLV, on the other hand, is due to the liquid crystal [11,12]. The undershoot and overshoot seen in the temporal response can be partially explained by a monotonic photoconductor response followed by the nonmonotonic static liquid crystal transfer curve. Experiments, however, indicate that this does not suffice as the entire explanation. A discussion of how this temporal response can be used to explain and predict system performance will be deferred to the next section.

1.2.4 Results

This section presents the experimental system used for demonstration of optical sequential logic along with results obtained thus far. The LCLV used in this system has a

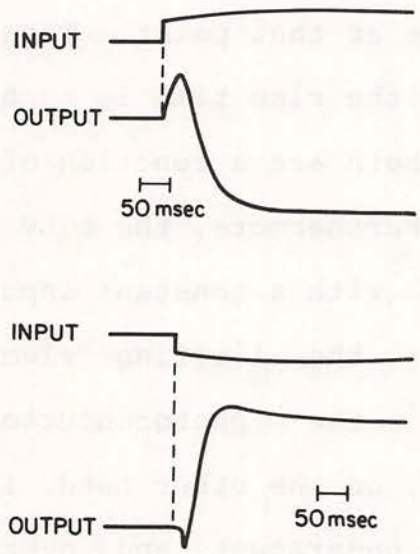

Fig. 11. Temporal response of LCLV to intensity-step input.

twisted-nematic liquid crystal layer with a total twist angle of 45 degrees. It is used in an inverting mode of operation to obtain the NOR function (Fig. 12). Interconnections are achieved with a computer-generated, space-variant hologram as described in section 1.2.2. The experimental system is shown in Fig. 13. A coherent, monochromatic beam is incident on the liquid crystal side of the LCLV, i.e., the gate output array, which is imaged onto the hologram and then Fourier transformed to yield the gate input array at the photoconductor side of the LCLV. Note that the system assures complete regeneration of spot location during each round trip and the mask at the hologram plane ensures regeneration of spot size. The system can be probed in two places without affecting its operation: (1) The gate output array can be seen using the reflection off the front surface of the hologram and (2) the gate input array appears in two diffracted orders at the LCLV, one of which is available for probing.

For purposes of demonstration, a test circuit needs to be chosen. A gate may be used in two different classes of circuits: (1) with feedback e.g. to achieve oscillation or memory, or (2) with no feedback. The requirements on the gate for proper functioning of the circuit may depend on which class of circuit is used. Thus a test circuit was chosen that includes both classes (Fig. 14). A hologram with the appropriate interconnection pattern was generated for this test circuit (Fig. 15). Some results of the operation of the system are shown in Figs. 16-18. The input and output intensity levels of a gate

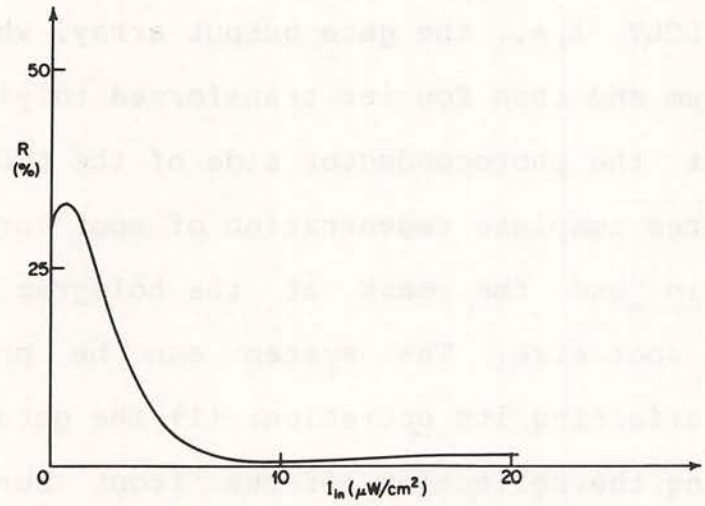

Fig. 12. Input-output characteristic of the twisted-nematic LCLV used in the experimental sequential logic system.

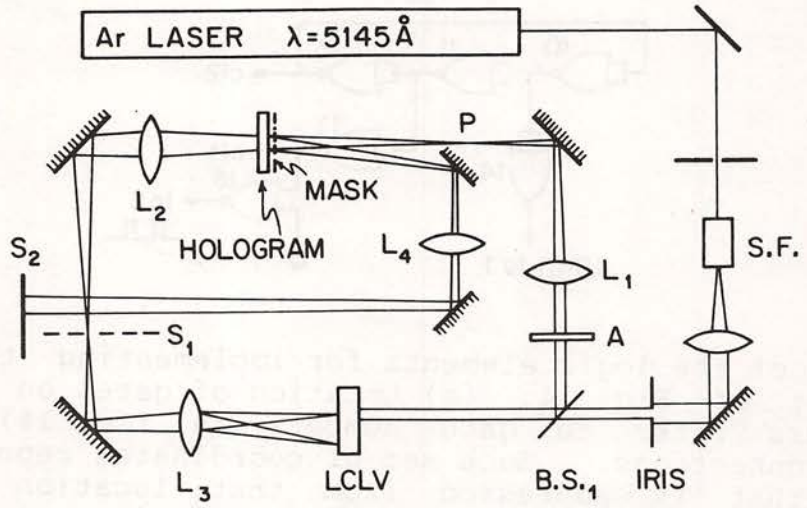

Fig. 13. Experimental setup for sequential logic using a reflective LCLV.

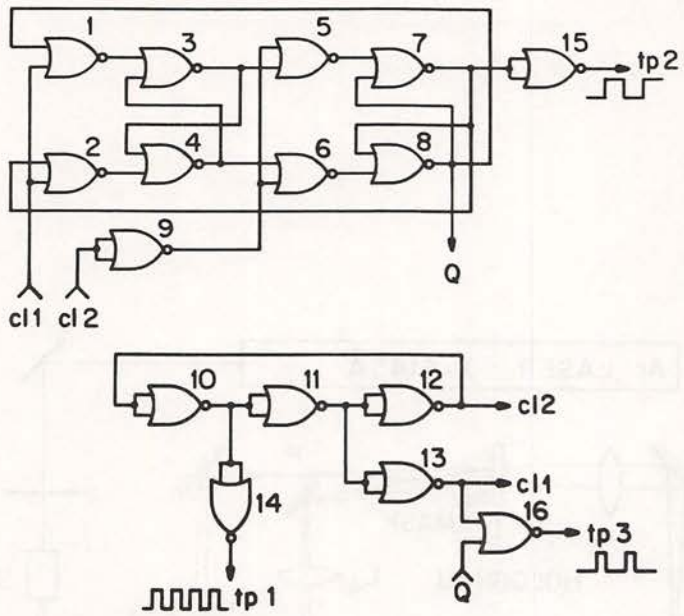

Fig. 14. Layout of the logic elements for implementing the test circuit of Fig. 14. (a) Location of gates on the LCLV (numbers refer to gate numbers in Fig. 14). (b) Interconnections. Each set of coordinates represents a gate that is addressed from that location in the hologram. A + indicates a double intensity value.

13	14	16	15
10	1	3	5
11	2	4	6
12	9	8	7

(A)

y \ x	1	2	3	4
1		tp 1	tp 3	tp 2
2	(3, 2) (2, 3) (2, 4)	(2, 1)+	(3, 1)+	(4, 1)+
3	(2, 2)+ (1, 4)+	(3, 3)	(4, 3) (3, 4)	(4, 5)
4	(1, 2)+ (1, 5)+	(3, 4)	(3, 3) (4, 4)	(3, 5)
5	(1, 3)+ (2, 5)+	(4, 3) (4, 4)	(2, 3 (3, 2) (4, 5)	(3, 5) (2, 4) (4, 2)+

(B)

Fig. 15. Input and output of a gate in the oscillator circuit. The period is a, the duty cycle is a/d, and the phase delay through the gate is 360 b/d.

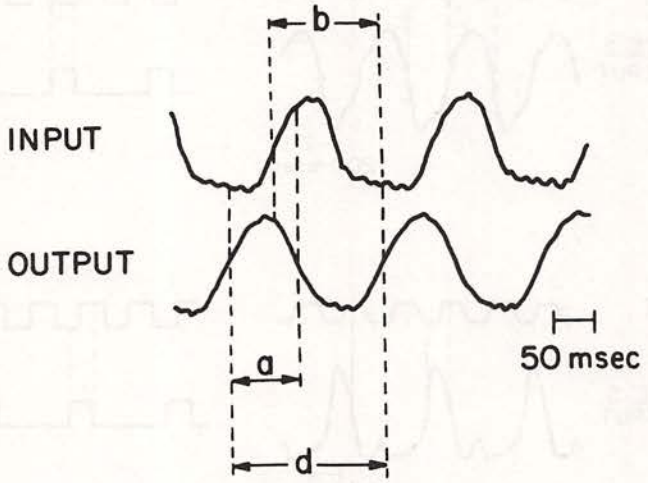

Fig. 16. Input and output of a gate in the oscillator circuit. The period is d, the duty cycle is a/d, and the phase delay through the gate is 360 b/d.

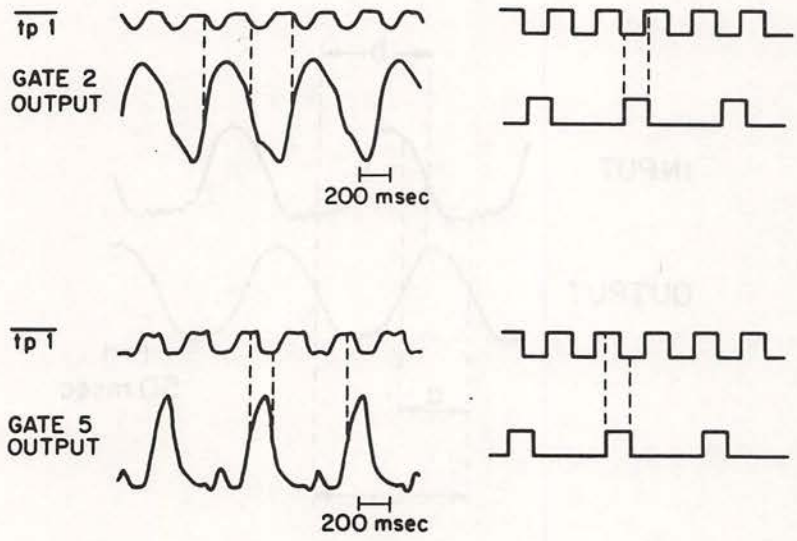

Fig. 17. Sample gate outputs in flip-flop circuit. Ideal outputs are shown to the right.

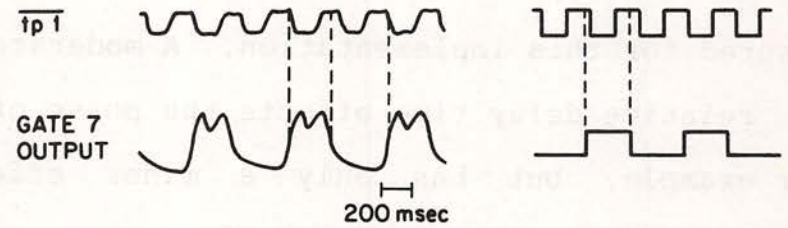

Fig. 18. Output of flip-flop circuit.

in the oscillator circuit appear in Fig. 16. The outputs of some of the other gates are shown in Figs. 17-18 along with timing diagrams representing the corresponding ideal outputs. The ideal outputs shown assume that the clock circuit pulse width is greater than four times the delay time introduced by one gate. The actual relationship between delay time and pulse width have not been measured for this implementation. A moderate change in the assumed relative delay time affects the phase of the output of gate 7 for example, but has only a minor effect on its waveshape. A large change in the delay time, however, could have a major effect on the shape or frequency of the wave.

In evaluating the experimental results, the circuit will be partitioned into two parts, each of which will be considered separately. The first part, consisting of the three gates that form the oscillator, will be discussed in the following three subsections.

1.2.4.1 Oscillator Circuit Behavior

Looking at the oscillator circuit behavior reveals that it is operating approximately as expected. Because of the feedback arrangement, the expected phase shift through a gate is 240 degrees, and the actual delay through the gate of Fig. 16 is approximately 256 degrees. The sum of the delays of the three oscillator gates was 720 degrees as expected. For gates of this type oscillating at their self-oscillating frequency, a waveform resembling a sinusoid is expected and is observed. The fact that

the duty cycle of the wave is not 50% can be explained by a difference in delay time for a rising and falling signal. Further insight into the behavior of the oscillator circuit can be gained by constructing a model, but in order to model the circuit, a model of the LCLV must first be developed.

1.2.4.2 LCLV Characteristic and Modeling

In the LCLV mode of operation used in this experiment, the voltage bias across the device is high enough for the liquid crystal molecules to act approximately as two uniform layers. The optical axis of the back layer is oriented at 45 degrees with respect to the front layer. Between the two layers the molecules are nearly perpendicular to the surfaces and therefore have little effect. As the write beam intensity is increased, the effective thickness of the two layers decreases, thus changing the integrated birefringence. A simple static model of the liquid crystal in this mode of operation consists of two equal thickness birefringent plates, the optical axis of each of which has been rotated 22.5 degrees on either side of vertical, and with a mirror as the back surface. Figure 19 shows the resulting intensity transmittance, as a function of integrated birefringence, when the device is placed between crossed polarizers. The write beam intensity increases from right to left on the graph. The LCLV is built to saturate at 0 or 2 on the horizontal axis. This model can be useful for predicting the output as parameters such as the total twist angle and the

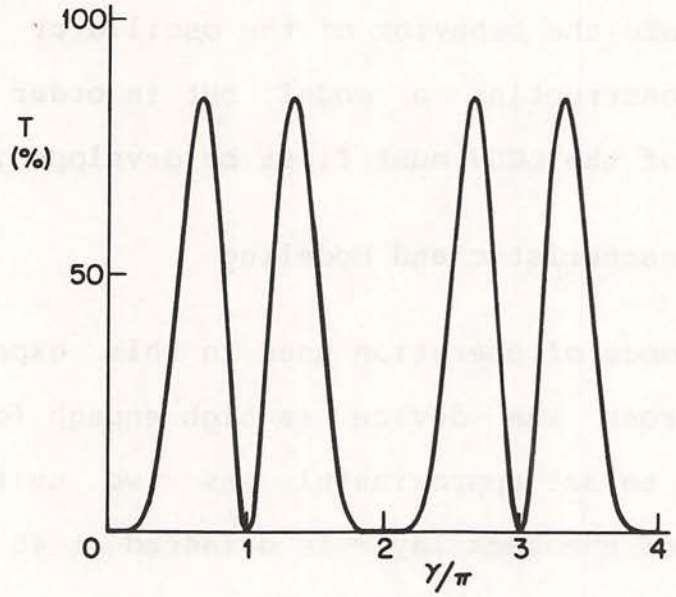

Fig. 19. Intensity transmittance T for a two-layer model of a 45 degree twisted nematic LC cell operating between crossed polarizers. γ is the integrated birefringence of each layer.

orientation of the input and output polarizers are varied. The accuracy of the model can be improved, as well as extended to give transmittance vs. write beam intensity, by using the LCLV model developed by Michaelson [11,12].

Turning now to time-dependent behavior, a model is needed for the temporal response of the LCLV for use in models of the circuits. The model considered here consists of a linear element, which introduces the time dependence, followed by a nonlinear element, which responds instantaneously (cf. section 1.2.3, last paragraph). A simple RC circuit is used for the linear element and an inverting, hard-clipping amplifier is used for the nonlinearity (Fig. 20). This model has been used to give rough predictions of LCLV behavior in the oscillator circuit. In order to incorporate some of the unusual temporal characteristics such as undershoot and overshoot, the amplifier can be replaced by the static LCLV input-output characteristic. An idea of the accuracy of this model using either nonlinearity may be obtained by comparing its response to a step input with that obtained experimentally.

Now that LCLV models have been presented, the discussion will turn back to the performance of the oscillator circuit.

1.2.4.3 Oscillator Circuit Models

Some basic information governing the behavior of the oscillator circuit may be obtained from a simple linear model of

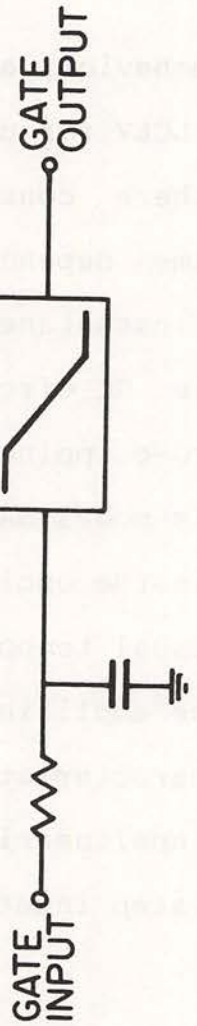

Fig. 20. Model for the temporal response of the LCLV.

each gate consisting of again an RC circuit, but this time followed by a linear inverting amplifier. The oscillator circuit with this model can be solved analytically. This solution allows us to draw three conclusions: (1) the condition for sustained oscillation is that the gain of the amplifier must be greater than 2, (2) the frequency of oscillation is proportional to the gain divided by the RC time constant, and (3) there is a 240 degree phase shift through each of the three gates. A numerical solution of the simple nonlinear model of Fig. 20 used in the oscillator circuit verifies statements (1) and (3), and is in approximate agreement with statement (2). It also gives an indication of the waveshape for various values of gain and amplifier cutoff levels (Fig. 21).

1.2.4.4 Flip-flop Circuit Results and Modeling

Turning our attention to the rest of the circuit, methods of analyzing it need to be studied in order to understand the outputs seen in Figs. 17 and 18.

First, the regeneration of the signal level at each pass through a gate will be considered. The general requirement is that a signal should not degenerate in passing through a large number of gates in series. Static considerations will be discussed first. Assuming a transition time of zero, the signal level at each pass through a gate may be read off the LCLV I/O curve. If f(x) represents this curve and x is the signal level at the gate input, then for the case of a simple inverter, the

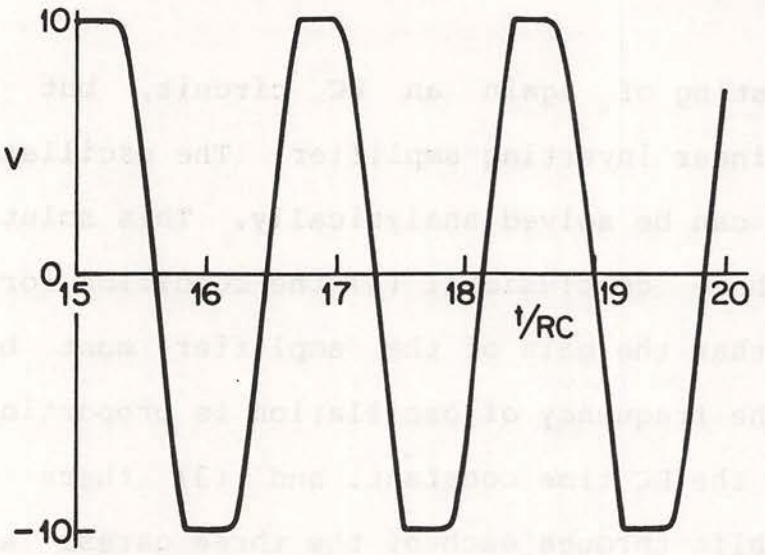

(a)

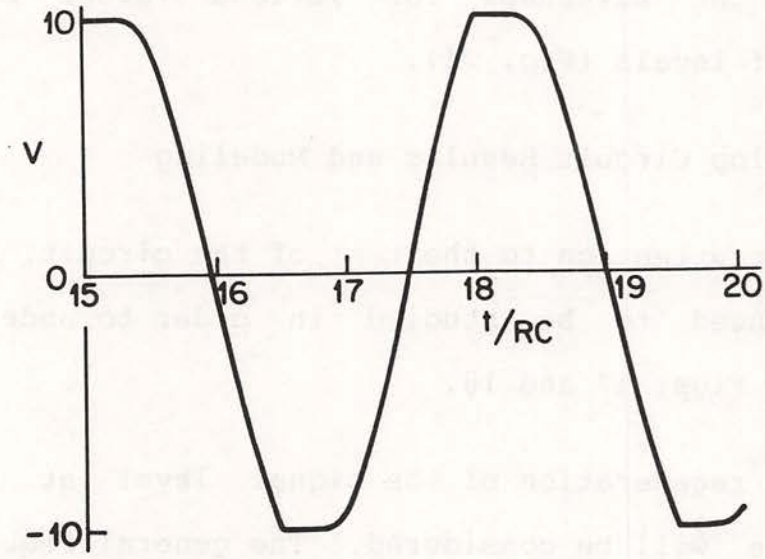

(b)

Fig. 21. Output V for a three stage feedback circuit, each stage of which is modeled by Fig. 20. The horizontal axis is measured in units of the RC time constant. The gain in each limiting amplifier is 5 in (a) and 2.5 in (b).

requirement

$$a_{1-i} < kf(x) < b_{1-i} \text{ for all } x \in (a_i, b_i),\ i=0,1 \qquad (10)$$

ensures that the signal will not degenerate. Here k is the gain from the output of one gate to the input of the next and $a_i < x < b_i$ defines the range of input signal levels interpreted as the discrete level i. These requirements are depicted in Fig. 22. This can easily be generalized to include the other Boolean operations. The I/O curve of the LCLV used in the experiment does satisfy these criteria for the NOR and NOT operations.

Having satisfied the static regeneration conditions, the temporal characteristics must be considered. Because of the unusual temporal response of the LCLV, the question of regeneration is not so easily answered. It can, however, be studied experimentally, by using the output of the oscillator circuit as an input to a long series of gates, and probing the signal at various points in the series. In addition, a separate input may be used, whose amplitude and frequency may be varied to determine the effects on the regeneration of the signal.

These investigations give us some guidelines on the device requirements which must be met to ensure proper operation in a binary circuit. These guidelines are not complete in their specification of the device performance. Therefore, modeling of the device in the circuit can be utilized to predict and analyze circuit performance with a given device.

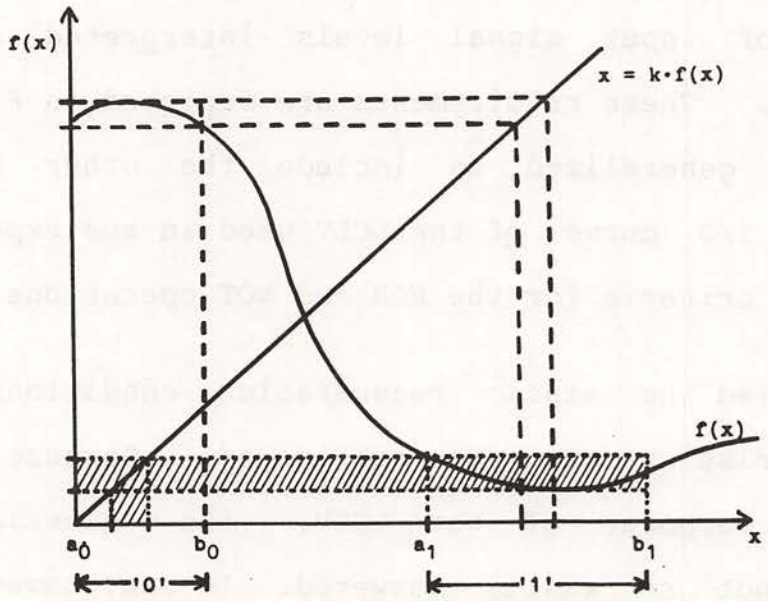

Fig. 22. Gate output, f(x), vs. gate input, x, for a curve that satisfies the steady-state regeneration criteria. The shaded region shows the criterion for a 1 input and a 0 output.

1.2.5 Conclusions

The present results indicate that the oscillator functions properly. The waveshapes and relative phases of the signals in the oscillator circuit were as expected. The final output of the circuit also agreed with the predicted waveform except for some relatively minor defects. However, the outputs of many of the other gates differ significantly from the expected waveshapes. These waveshapes will be improved through an experimental study of the temporal regeneration of the signal and through device modeling applied to the circuit. This should yield waves that have approximately the expected duty cycles and do not have the spurious pulses that the present results exhibit.

1.3 Variable Grating Mode Liquid Crystal Devices: Modeling

The variable grating mode (VGM) liquid crystal device has been further studied experimentally [13-21]. This work has been in conjunction with the device development work being done at Hughes Research Laboratories.

An important area of research on the Variable Grating Mode Liquid Crystal Light Valve is concerned with a fundamental understanding of the origin of the "variable grating" effect. A wide variety of studies have been performed on electrically addressed VGM cells (no intervening photoconductive layer), in which diffraction order polarization and intensity were measured as a function of input polarization and applied cell voltage and the results correlated with observations of the VGM structure under polarized illumination in a polarizing microscope, as well as the with various theoretical models of the VGM domain structure.

Extremely interesting results have been obtained from this investigation, which suggest the absolute spatial configuration of the liquid crystal director. For all input polarization conditions, the even and odd diffraction orders are found to be essentially linearly polarized. In addition, the even diffraction orders are nearly linearly polarized parallel to the domains comprising the VGM grating, as shown in Fig. 23. For input polarization perpendicular to the domains, all even orders are found to be almost completely extinguished. On the other

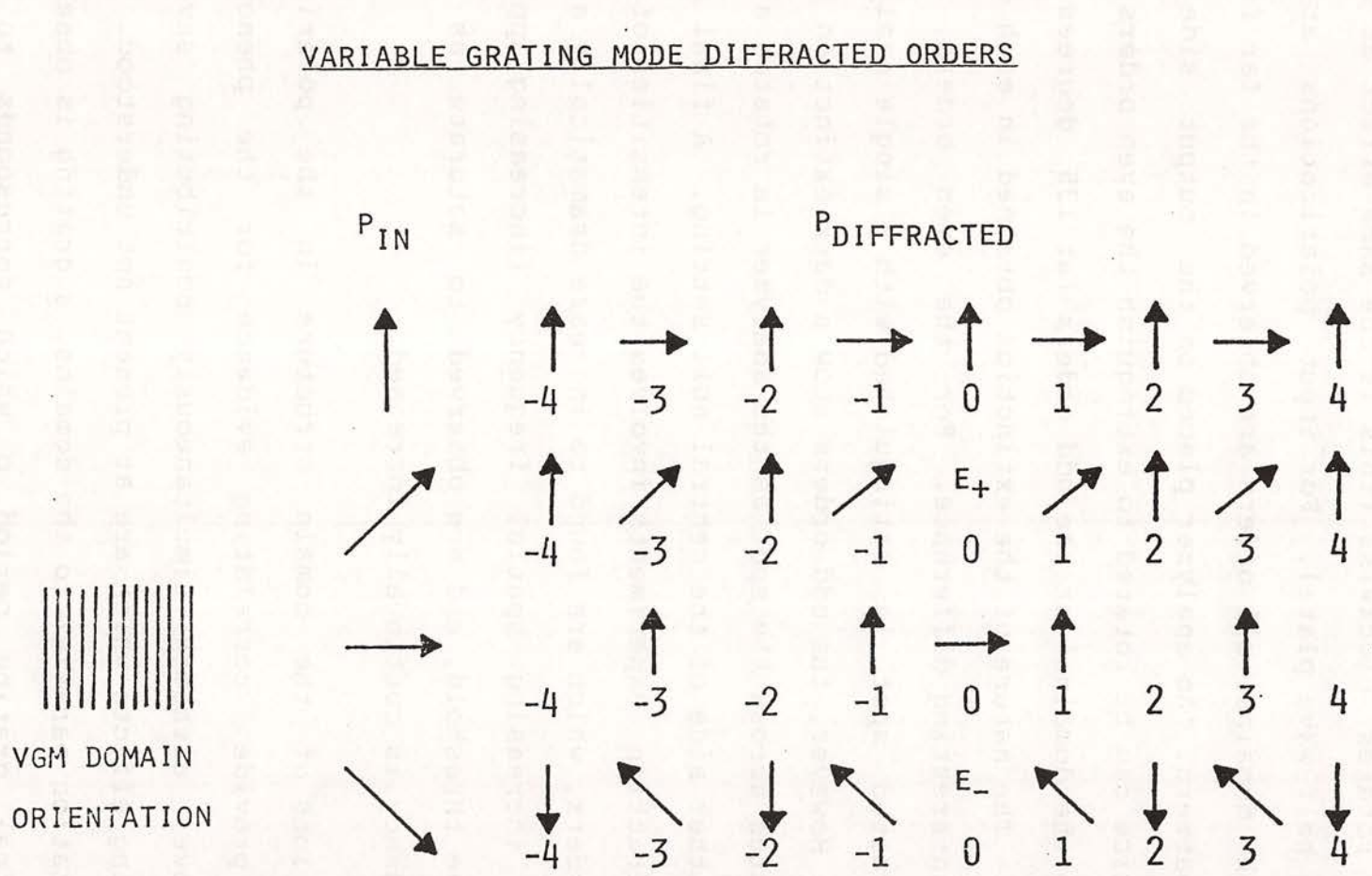

Fig. 23 Polarization behavior of VGM diffraction orders. The left-hand column indicates input polarization, the top row indicates diffraction order and the other entries indicate corresponding output polarization.

hand, the odd diffraction orders are always linearly polarized with a major axis that rotates counterclockwise as the input polarization rotates clockwise (this is the same effect as that produced by a half-wave plate). For input polarizations at 45 degrees to the domains, all orders are observed in the far field diffraction pattern. An analyzer placed on the output side of the VGM device can be rotated to extinguish the even orders (at 90 degrees to the domains) or the odd orders (at 135 degrees to the domains). The nature of the extinction obtained in each case exhibits an interesting difference. For the even orders, the entire diffracted spot is extinguished with a single analyzer orientation. However, the odd orders show a dark extinction band that propagates across the spot as the analyzer is rotated a few degrees to either side of the central null setting. A final note on the diffraction experiments involves the intensities of the diffracted orders, which are found to increase dramatically as a function of increasing spatial frequency (increasing applied voltage) above threshold, and are observed to saturate as the spatial frequency is continually increased.

Observations of the domain structure in the polarizing microscope provide correlating evidence for the phenomena described above, although simultaneously contributing several other puzzling effects which are at present not understood. For input polarization parallel to the domains, a grating is observed with principal grating period p which corresponds to the diffraction angle of the second order. For input polarization

perpendicular to the domains, a grating is observed with period 2p, which corresponds to the diffraction angle of the first order. Other input polarization orientations produce apparent superposition of the p and 2p gratings, in agreement with the diffraction experiment results. The above described experiments are performed with the focus set at the upper interior ITO-coated glass substrate surface. The domain contrast can be altered, and in some cases reversed by adjusting the focal plane to lie within the liquid crystal layer. The origin of this effect is under continuing investigation.

A number of domain discontinuities can be observed within the liquid crystal layer, similar in appearance to crystallographic dislocations. The dislocation density increases with time as each VGM device cell deteriorates. As the applied bias across an electrically activated cell is increased or decreased, the dislocations propagate past each other while the domain period decreases or increases, respectively. Dislocations with opposite orientations propagate in opposite directions until a new stable equilibrium situation is achieved. It is not yet clear whether these dislocations represent true disclinations, in which the liquid crystal director is undefined near a discontinuity, or whether they are merely alternative local continuous solutions to the free energy minimization.

A periodic uniaxial birefringence model specifying the liquid crystal director as a function of spatial position has

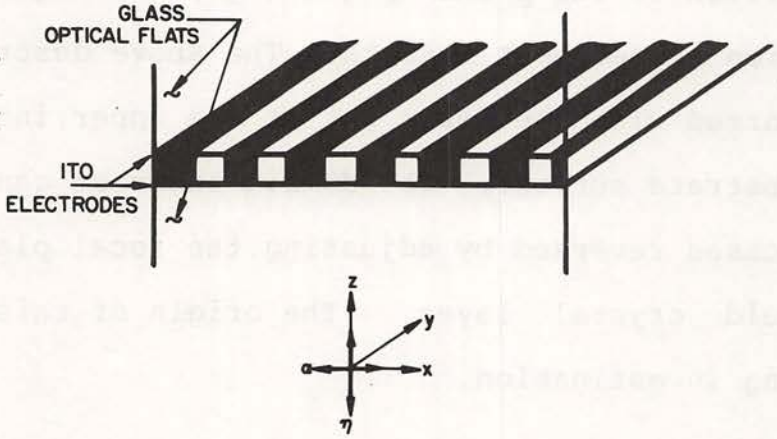

Fig. 24 Definition of VGM geometry and coordinates. α is a tilt angle in the plane of the VGM layer and η is the tilt angle out of the plane.

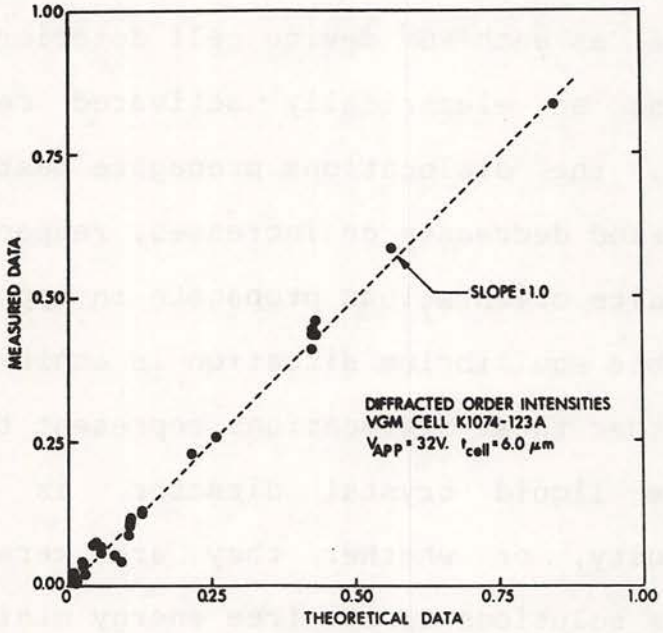

Fig. 25 Measured diffraction efficiencies as a function of calculations of expected diffraction efficiencies based on the model of the VGM molecular orientation. A perfect fit of experiment to theory would be indicated if all data points fell on 45° line.

been derived that explains the majority of the above observations. A key feature of this model is the inclusion of both phase and birefringent phase grating contributions to the total polarization dependent diffraction efficiency. The model specifies the spatial dependence of the angular orientation of the liquid crystal molecules within a domain in terms of an in-plane rotation angle (α) and an out-of-plane rotation angle (η) as shown in Fig. 24. The Fourier transform of the amplitude distribution of light emergent from the VGM cell gives the far-field diffracted order pattern. Measured values of order intensities as functions of input and output polarization at a given cell voltage and thickness were compared with theoretical predictions from the model for various combinations of orientation angle pairs (α,η) in order to determine the optimum RMS fit at each applied voltage. In a 6 micron thick cell at V_{app}=32V, the fit is excellent as shown in Fig.25.This procedure allows the extraction of the maximum orientational excursion angles $\alpha(V)$ and $\eta(V)$ as a function of applied bias, as shown in Figs. 26 through 29. Over the limited voltage (spatial frequency) range examined to date, both α and η appear to be linear functions of the logarithm of the voltage across the cell.

In order to refine the theoretical model, efforts have been made to include an appropriate thickness dependence of the liquid crystal director within the liquid crystal layer. In the model described above, the liquid crystal director has been assumed to be characterizable by orientation angles α and η that vary in the

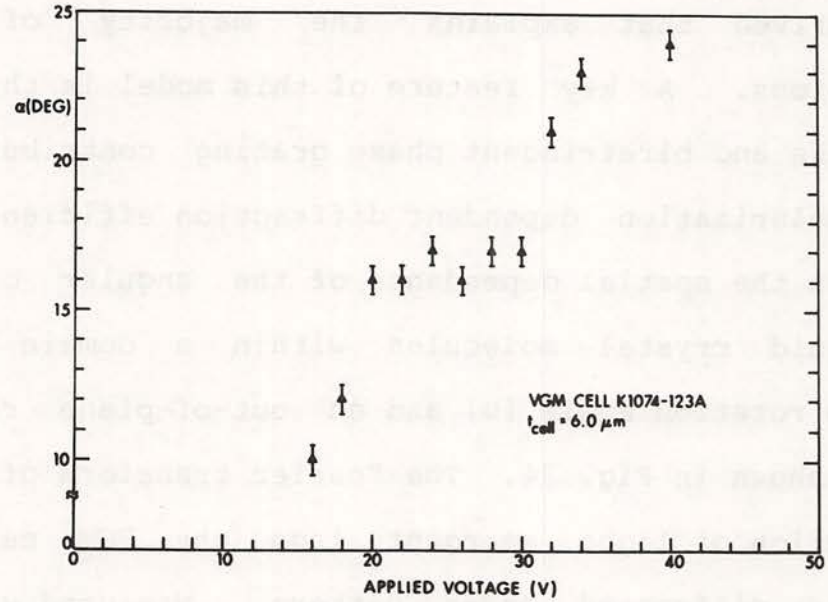

Fig. 26 Maximum in-plane angle α_{max} versus applied voltage.

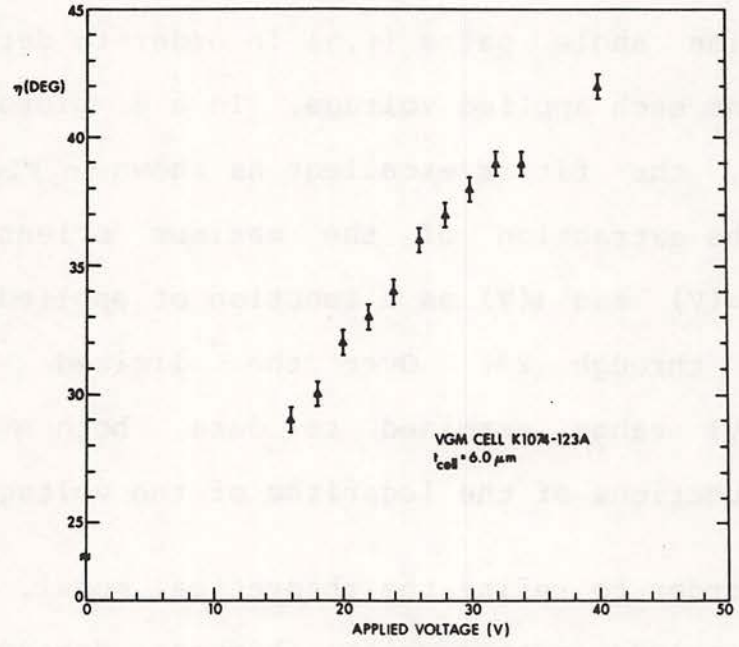

Fig. 27 Maximum out-of-plane angle η_{max} versus applied voltage.

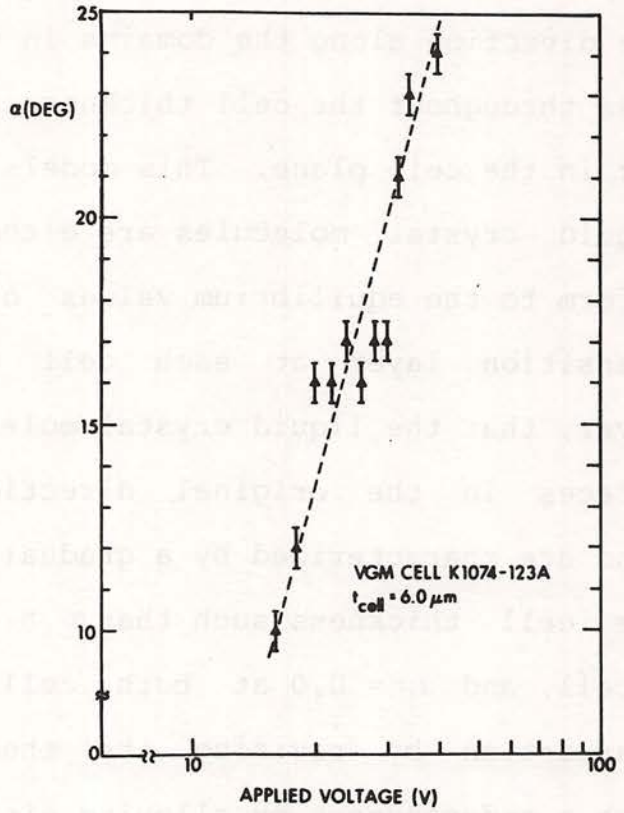

Fig. 28 α_{max} versus log (V)

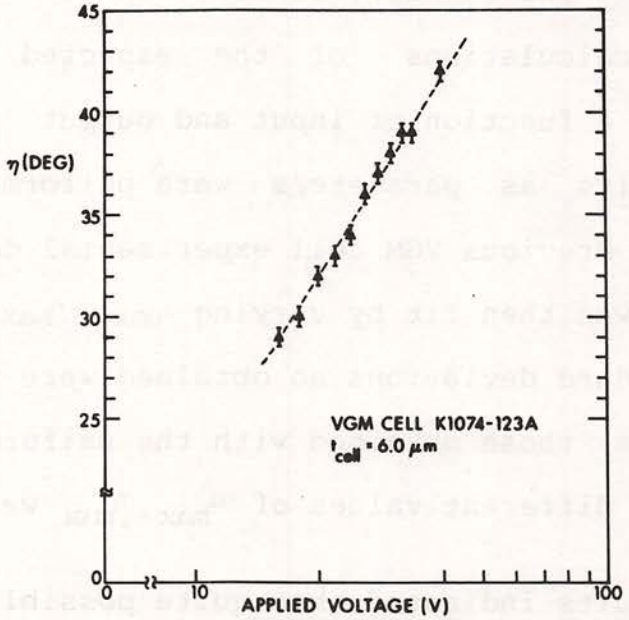

Fig. 29 η_{max} versus log (V)

direction normal to the domains in the plane of the cell, but are constant in the direction along the domains in the plane of the cell as well as throughout the cell thickness at a given spatial coordinate pair in the cell plane. This models a situation in which the liquid crystal molecules are either unpinned at the surface, or deform to the equilibrium values of α, η through a very thin transition layer at each cell interface. It is possible, however, that the liquid crystal molecules <u>are</u> pinned at the interfaces in the original direction of preferential orientation, and are characterized by a gradual distortion in α, η throughout the cell thickness such that $\alpha, \eta = \alpha_{max}, \eta_{max}$ at the center of the cell, and $\alpha, \eta = 0,0$ at both cell interfaces. We tested this assertion by revising the theoretical model to incorporate such a z-dependence by allowing either α, η, or both to vary throughout the cell thickness as $\alpha(z) = \alpha_{max} \sin kz$ where $k = \pi/d$ to satisfy the boundary conditions $\alpha(0) = 0$ and $\alpha(d) = 0$. Theoretical calculations of the expected diffracted order intensities as a function of input and output polarization with α_{max}, η_{max} pairs as parameters were performed subject to this modification. Previous VGM cell experimental data (that shown in Figs. 26-29) was then fit by varying α_{max}, η_{max} for the best RMS fit. The standard deviations so obtained were not significantly different from those obtained with the uniform thickness model, although quite different values of α_{max}, η_{max} were obtained.

These results indicated that quite possibly these two models were in fact isomorphic. were attempted

in order to match a given set of theoretical values of diffracted order amplitudes from the uniform model, with those from the nonuniform sine model, using $\alpha_{max,sine}$;$\eta_{max,sine}$ as parameters in achieving the best RMS fit. Such attempts always showed significant differences in the higher diffracted orders. Theoretical analysis of simplified cases showed that in fact these two models are not isomorphic, although they are quite similar in many respects. The data set we have generated thus far is not precise enough to allow differentiation between these two models. Further experimental and theoretical efforts designed to elucidate this behavior are the substance of ongoing research.

Numerous experimental measurements of the off-diagonal elements in the Jones matrix describing polarized light propagation through the VGM cell have revealed a significant asymmetry not predicted by the uniaxial model. The origin of this "B/C asymmetry" effect is under continuing investigation.

A free energy minimization calculation for static (dc) VGM along the lines of similar calculations in de Gennes [22] has been performed in order to identify critical parameters affecting the formation of VGM domains. We obtain (independently) a solution under assumptions related to electric field induced piezoelectric instability that agrees in most respects with our experimental observations (principally the spatial evolution of the orientational angles α,η). This solution is also quoted by

Bobylev and Pikin [23], based on earlier work by Meyer [24]. Using reasonable values of our VGM liquid crystal parameters, the dependence of grating frequency on applied electric field can be derived, which agrees rather well with our experimental results to date [18,19,21]. This is a very important development, as it lends credence to our phenomenologically derived orientational configuration, and provides considerable insight into the fundamental origins of the VGM effect. Further investigation along these lines will hopefully allow optimization of the VGM domain formation response time.

1.4 Variable Grating Mode Liquid Crystal Devices: Applications

The VGM device fundamentally performs a two-dimensional local intensity-to-spatial frequency inversion. Several new areas of application for VGM devices have recently been explored, including nonlinear point intensity transformations [13] optical combinatorial logic functions [14], and digital circuits such as a full adder.

One of the nonlinear point operations originally implemented on early versions of the VGM device was a level slice function [13]. This operation is simple because the required spatial filter is a slit that passes a limited band (or bands) in the spatial frequency domain. Recent improvements in VGM device technology and fabrication have been made, and this level slice experiment was repeated with an improved device.

The experimental setup is similar to that used in previous level slice experiments. The input image is illuminated by an arc lamp source and imaged onto the photoconductor surface of the VGM device. The VGM device has a dc bias voltage that produces a uniform phase grating structure with no illumination. The grating period is locally modulated by the input picture intensity, and this modulation is mapped into a position along a line in the spatial frequency plane. A red filter ensures that only the readout laser beam enters the coherent optical processor. Small circular annuli of varying radii are used to pass certain spatial frequency bands. This effectively allows

only prescribed input ranges to appear in the output. Figure 30 shows the input and level sliced output pictures. Figure 30a shows the original input image in positive print form; a negative of the original was used in the experiment. Figure 30b-i shows the level slice outputs obtained in sequence as the transmitting annulus is adjusted to transmit progressively lower spatial frequencies. Thus the level slice sequence begins with the highest intensity level in Fig. 30b and proceeds to the lowest level slice in Fig. 30i.

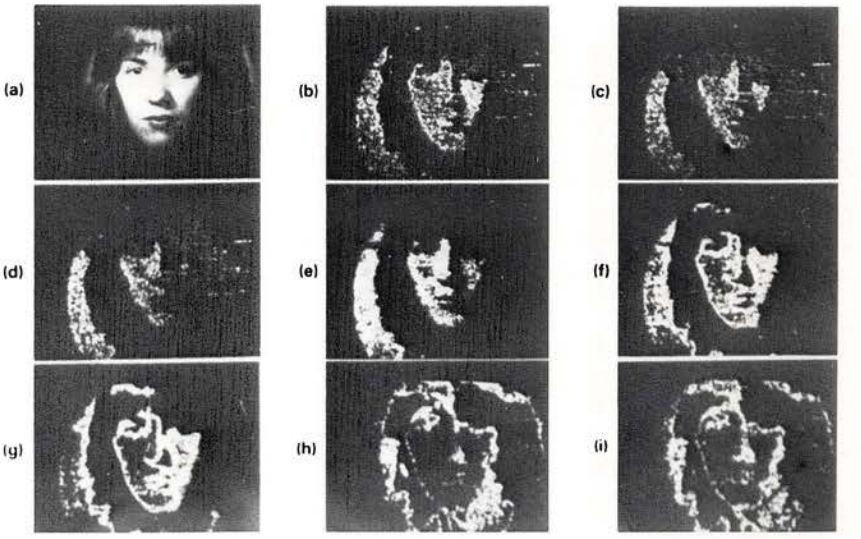

Fig. 30. Variable level slice with VGM device. (a) is the original input pattern and (b)-(i) represent level slice outputs obtained by moving the slit location in the filter plane.

1.5 References

1. A.A. Sawchuk and T.C. Strand, "Fourier Optics in Nonlinear Signal Processing," Ch 9 of Applications of Optical Fourier Transform, H. Stark, ed., Academic, New York, 1981.

2. A.A. Sawchuk, T.C. Strand, and A.R. Tanguay, Jr., "Nonlinear Real-Time Optical Signal Processing," Final Technical Report for Grant No. AFOSR-77-3285, Report USCIPI 1020, USC Image Processing Institute, Los Angeles, Ca. 90089, June 1981.

3. A. Armand, A.A. Sawchuk, T.C. Strand, B.H. Soffer and D. Boswell, "Real-time Parallel Optical Analog-to-Digital Conversion," Optics Letters, vol. 5, pp. 129-131, 1980.

4. P. Chavel, A.A. Sawchuk, T.C. Strand, A.R. Tanguay, Jr., and B.H. Soffer, "Optical Logic with Variable-Grating-Mode Liquid-Crystal Devices," Optics Letters, vol. 5, pp. 398-400, 1980.

5. A.W. Lohmann, D.P. Paris, "Binary Faunhofer Holograms, Generated by Computer," Applied Optics, vol. 6, p. 1739, 1967.

6. W.H. Lee, "Sampled Fourier Transform Hologram Generated by Computer," Applied Optics, vol. 9, p. 639, 1970.

7. C.B. Burckhardt, "A Simplification of Lee's Method of Generating Holograms by Computer," Applied Optics, vol. 9, p. 1949, 1970.

8. C.K. Hsueh, A.A. Sawchuk, "Computer-Generated Double-Phase Holograms," Applied Optics, vol. 17, p. 3874, 1978.

9. J. Fleuret, "Contributions to Numerical Holography: Three Different Applications," in Applications of Holography and Optical Data Processing, Proceedings of the I.C.O. Conference, Jerusalem, Israel, 23-26 Aug. 1976, E. M.Marom, A.A. Friesem, E. Wiener-Avnear, ed., Pergamon Press, Oxford, 1977.

10. J. Bucklew, N. Gallagher, Jr., "Comprehensive Error Models and a Comparative Study of Some Detour-Phase Holograms," Applied Optics, vol. 18, p. 2861, 1979.

11. J.D. Michaelson, "Characterization of Liquid Crystal Light Valves and Their Applications to Real-Time Nonlinear Optical Processing," Ph.D. Thesis, Department of Electrical Engineering, University of Southern California, Los Angeles, 1979.

12. J.D. Michaelson, "A First-Order Model of a Photo-Activated Liquid Crystal Light Valve," Proc. SPIE Devices and Systems for Optical Signal Processing, vol. 218, pp. 88-95, 1980.

13. B.H. Soffer, J.D. Margerum, A.M. Lackner, D. Boswell, A.A. Sawchuk, T.C. Strand, A.R. Tanguay, Jr., and P. Chavel, "Variable Grating Mode Liquid Crystal Device for Optical Processing and Computing," Molecular Crystals and Liquid Crystals, vol. 70, pp. 145-161.

14. A.A. Sawchuk, "Intensity-to-spatial Frequency Transformations," Proceedings Society of Photo-Optical Instrumentation Engineers Advanced Institute of Transformations in Optical Signal Processing, Seattle, (February 1981).

15. A.A. Sawchuk, "Recent Developments in Optical and Digital Processing," Proceedings Workshop on Optical Information Processing, Centro de Investigaciones en Optica, Cuernavaca, Mexico, (January 1982).

16. A.R. Tanguay, Jr., P. Chavel, T.C. Strand, J. Wu, and B.H. Soffer, "Physical Characterization of the Variable Grating Model Liquid Crystal Devices," SPIE Proc. Advances in Optical Information Processing, vol. 388, (January 1983).

17. A.R. Tanguay, Jr., P. Chavel, T.C. Strand, and J.S. Wu, "Polarization Properties of the Variable Grating Mode Liquid Crystal Device," to be submitted to Applied Optics.

18. A.R. Tanguay, Jr., T.C. Strand, P. Chavel, A.A. Sawchuk, and B.H. Soffer, "Theoretical and Experimental Polarization Properties of the Variable Grating Mode Liquid Crystal Structure," presented at 1981 Annual Meeting, Optical Society of America, Orlando, Florida, October 1981, Journal of the Optical Society of America, vol. 71, p. 1630, (December 1981).

19. A.R. Tanguay, Jr., "Recent Progress in Spatial Light Modulators for Coherent Optical Processing Applications," 1982 Gordon Conference on Holography and Optical Information Processing, Plymouth, New Hampshire, 1982.

20. A.R. Tanguay, Jr., "Polarization Properties of Birefringent Phase Gratings," presented at 1982 Annual Meeting, Optical Society of America, Tucson, Arizona, October 1982: Journal of the Optical Society of America, vol. 72, (1982).

21. A.R. Tanguay, Jr., "Spatial Light Modulators for Real Time Optical Processing," Proc. ARO Workshop on Future Directions for Optical Informtion Processing, pp. 52-76, Lubbock, Texas, May, 1980.

22. P.G. de Gennes, The Physics of Liquid Crystals Claredon Press, Oxford, (1975).

23. Yu P. Bobylev and S.A. Pikin, "Threshold Piezoelectric Instability in a Liquid Crystal," Sov. Phys. JETP, vol. 45,

pp. 195-198, (1977).

24. R.B. Meyer, Phys. Rev. Lett., vol. 22, 918, (1969).

25. P. Auborg, J.P. Huignard, N. Hareng, and R.A. Mullen, "Liquid Crystal Light Valve Using Bulk Monocrystalline $Bi_{12}SiO_{20}$ as the Photoconductive Material," Appl. Opt., vol. 21, 3706-3711, (1982).

2. PROFESSIONAL PERSONNEL

The following individuals contributed to the research effort supported by this grant since its beginning in April 1981:

1. Alexander A. Sawchuk, Professor, Department of Electrical Engineering, Director - Image Processing Institute, Principal Investigator.

2. Timothy C. Strand, Research Assistant Professor, Image Processing Institute, Senior Investigator.

3. Armand R. Tanguay, Jr., Assistant Professor, Departments of Electrical Engineering and Materials Science, and Image Processing Institute, Senior Investigator.

4. Pierre H. Chavel, Visiting Research Scientist, Image Processing Institute (on leave from Institut d'Optique, Orsay, France).

5. Robert Forchheimer, Visiting Research Scientist, Image Processing Institute (on leave from Linkoping University, Linkoping, Sweden).

6. Keith Jenkins, Research Assistant, Ph.D. Candidate, Department of Electrical Engineering.

7. John Wu, Research Assistant, Ph.D. Candidate, Department of Electrical Engineering.

3. PUBLICATIONS

This section lists written publications resulting from AFOSR support of this project from the April 15, 1981 starting date.

1. A.A. Sawchuk and T.C. Strand, "Fourier Optics in Nonlinear Signal Processing," Ch. 9 of Applications of Optical Fourier Transforms, H. Stark, ed., Academic, New York, (1981).

2. A. Armand, A.A. Sawchuk and T.C. Strand, "Nonlinear Optical Processing with Halftones: Accurate Predictions for Degradation and Compensation," to be submitted to Applied Optics.

3. A. Armand, A.A. Sawchuk, T.C. Strand, and B.H. Soffer, "Real-Time Parallel Logarithmic Filtering," Optics Letters, vol. 7, pp. 451-453, (September 1982).

4. B.H. Soffer, J.D. Margerum, A.M. Lackner, D. Boswell, A.A. Sawchuk, A.R. Tanguay, Jr., T.C. Strand, and P. Chavel, "Variable Grating Mode Liquid Crystal Device for Optical Processing and Computing," Molecular Crystals and Liquid Crystals, vol. 70, pp. 145-161, (1981).

5. A.A. Sawchuk, "Intensity-to-Spatial Frequency Transformations," Proceedings Society of Photo-Optical Instrumentation Engineers Advanced Institute on Transformations in Optical Signal Processing, Seattle, (February 1981).

6. A.A. Sawchuk, "Recent Developments in Optical and Digital Processing," Proceedings Workshop on Optical Information Processing, Centro de Investigaciones en Optica, Cuernavaca, Mexico, (January 1982).

7. A.R. Tanguay, Jr., P. Chavel, T.C. Strand, J. Wu, and B.H. Soffer, "Physical Characterization of the Variable Grating Model Liquid Crystal Device," SPIE Proc. Advances in Optical Information Processing, vol. 388, (January 1983), to appear.

8. A.R. Tanguay, Jr., P. Chavel, T.C. Strand, and J.S. Wu, "Polarization Properties of the Variable Grating Model Liquid Crystal Device," to be submitted to Applied Optics.

9. P. Chavel, R. Forchheimer, B.K. Jenkins, A.A. Sawchuk, and T.C. Strand, "Architectures for a Sequential Optical Logic Processor," Proceedings 10th International Optical Computing Conference, Cambridge, Ma., (April 1983), to appear.

4. ORAL PRESENTATIONS

This section lists oral presentations at meetings and conferences describing research supported by this grant from the April 15, 1981 starting date.

1. A.R. Tanguay, Jr., T.C. Strand, P. Chavel, A.A. Sawchuk, and B.H. Soffer "Theoretical and Experimental Polarization Properties of the Variable Grating Model Liquid Crystal Structure," presented at 1981 Annual Meeting, Optical Society of America, Orlando, Florida, October 1981, Journal of the Optical Society of America, vol. 71, p. 1630, (December 1981).

2. A.R. Tanguay, Jr., "Recent Progress in Spatial Light Modulators for Coherent Optical Processing Applications," 1982 Gordon Research Conference on Holography and Optical Information Processing, Plymouth, New Hampshire, (1982), (Invited Paper).

3. A.R. Tanguay, Jr., "Polarization Properties of Birefringent Phase Gratings," 1982 Gordon Research Conference on Holography and Optical Information Processing, Plymouth, New Hampshire, (1982), (Invited Paper).

4. B.K. Jenkins, A.A. Sawchuk, T.C. Strand, and B.H. Soffer, "Sequential Optical Logic Implementation," presented at 1982 Annual Meeting, Optical Society of America, Tucson, Arizona, October 1982; Journal of the Optical Society of America, vol. 72, (1982).

5. A.R. Tanguay, Jr., "Polarization Properties of Birefringent Phase Gratings," presented at 1982 Annual Meeting, Optical Society of America, Tucson, Arizona, October 1982; Journal of the Optical Society of America, vol. 72, (1982).